Real-Time Observation of the Regime Transition Dynamics of Mode-Locked Fiber Lasers

Guoqing Pu, Lilin Yi, Li Zhang, Yuanhua Feng, Zhaohui Li, and Weisheng Hu

***Abstract*— Mode-locked lasers exhibit complex nonlinear dynamics. Precise observation of these dynamics will aid in the understanding of the underlying physics and provide new insights for laser design and applications. The starting dynamics, from initial noise fluctuations to the mode-locking regime, have previously been observed directly by time-stretched transform-based real-time spectroscopy. However, the regime transition dynamics, which are essential processes in mode-locked lasers, have not yet been resolved because regime transition process tracking is very challenging. Here we demonstrate the real-time observation of the regime transition dynamics enabled by our design of a real-time programmable mode-locked fiber laser, in which different operating regimes can be achieved and switched automatically. The regime transition dynamics among initial noise fluctuations, Q-switching, fundamental mode-locking and harmonic mode-locking regimes have been observed and thoroughly analyzed by both temporal and spectral means. These findings enrich our understanding of the complex dynamics inside mode-locked lasers.**

***Index Terms*— Mode-locked fiber lasers, time-stretch, ultrafast dynamics.**

I. Introduction

THE internal dynamics of mode-locked fiber lasers (MLFLs) are attractive for various applications of MLFLs [1]. Recently, several researchers have investigated these dynamics using the time-stretch dispersive Fourier transform (TS-DFT) [2]. Through a dispersive medium, the TS-DFT builds up a mapping from the spectrum to the temporal domain pulse and a real-time optical spectrum analysis can be performed by combining the TS-DFT with a real-time oscilloscope [3]. The TS-DFT provides endless possibilities for comprehension of ultrafast physical phenomena, including optical rogue waves [4], soliton explosions [5], mode-locking build-up processes [6]–[8] and sophisticated soliton dynamics [9]–[11]. The mode-locking build-up process of a Kerr-lens Ti: sapphire laser [6] was successively resolved. The mode-locking build-up processes in an anomalous dispersion fiber laser [7] and the build-up dynamics of a dissipative soliton [8] have also been observed. In addition, the complete build-up dynamics of soliton molecules [10] and soliton dynamics related to Q-switched instabilities [11] in MLFLs have also been investigated. However, all these observations are without exception based on the pulse build-up processes that are induced by increasing the pump power. There has been no possibility to date of observation of the pulse transition dynamics from one mode-locking regime to another; these transitions are essential physical processes in MLFLs but tracking of the regime transition process is very challenging. Because regime transitions are very difficult to realize using pump power tuning alone. Therefore, studies of the nonlinear dynamics of MLFLs are not yet complete.

Nonlinear polarization evolution (NPE) is the main method that is used to achieve mode locking. In addition to the fundamental mode-locking (FML) regime, NPE-based MLFLs can also produce harmonic mode-locking (HML) regime with high repetition rates [12] and Q-switching (QS) regime with high pulse energies [13], [14] by polarization tuning alone. Therefore, NPE-based MLFLs represent the perfect platform for investigation of the regime transition dynamics. We have previously designed the first real-time programmable MLFL using intelligent polarization tuning that can be automatically locked on and switched among the QS, Q-switched mode-locking (QML), FML and HML regimes [15]. In this letter, by virtue of this real-time programmable MLFL with a combination of temporal and spectral observations obtained using the TS-DFT and a real-time oscilloscope, we first reveal the QS and mode-locking build-up processes induced by polarization tuning. Furthermore, we provide the real-time observation of the regime transition dynamics among the QS, FML and HML regimes probed by polarization tuning. Our observations have demonstrated some interesting findings that have not been reported previously. For example, the regime transition from QS to stable FML experiences dual-wavelength competition. The formation processes for QS pulses are quite similar, regardless of whether they are built up from the initial noise fluctuations or transited from the FML regime, in which dual-envelope competition always exists and only the dominant pulse can eventually be oscillated. The transition from FML to the HML regime will require tens of thousands of roundtrip times to achieve stable spectral operation, but the reverse transition only requires tens of roundtrip times to achieve stable operation, corresponding to a regime switching time as fast as tens of microseconds. We believe that these interesting findings provide researchers with a better understanding of the

Manuscript received July 15, 2019; revised August 10, 2019; accepted August 18, 2019. Date of publication August 21, 2019; date of current version September 10, 2019. This work was supported by the National Natural Science Foundation of China under Grant 61575122. *(Corresponding author: Lilin Yi.)*

G. Pu, L. Yi, L. Zhang, and W. Hu are with the State Key Laboratory of Advanced Optical Communication Systems and Networks, Shanghai Jiao Tong University, Shanghai 200240, China (e-mail: lilinyi@sjtu.edu.cn).

Y. Feng is with the Department of Electronic Engineering, College of Information Science and Technology, Jinan University, Guangzhou 510632, China.

Z. Li is with the School of Electronics and Information Technology, Sun Yat-sen University, Guangzhou 510006, China (e-mail: lzhh88@mail.sysu.edu.cn).

Color versions of one or more of the figures in this letter are available online at http://ieeexplore.ieee.org.

Digital Object Identifier 10.1109/LPT.2019.2936578

1041-1135 © 2019 IEEE. Personal use is permitted, but republication/redistribution requires IEEE permission.
See http://www.ieee.org/publications_standards/publications/rights/index.html for more information.

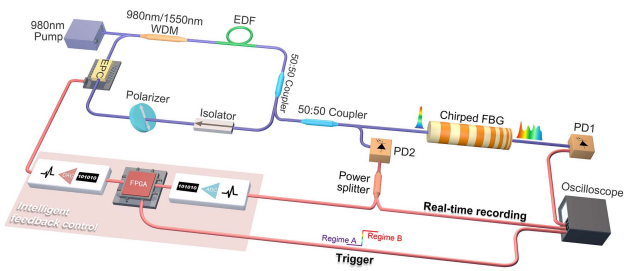

Fig. 1. Experimental setup.

internal dynamics of MLFLs and thus aid in the design and application of these lasers.

II. Principles

Figure 1 illustrates the complete experimental setup, where the left side shows the real-time programmable MLFL that was enabled by our proposed intelligent algorithm [15]. A 980 nm laser with a fixed power of 600 mW pumps an 8 m erbium-doped fiber (EDF) with the dispersion of −38 ps/nm/km as the gain medium through a wavelength division multiplexer (WDM). The isolator guarantees unidirectional running and the polarizer is the key component for NPE-based mode-locking. An electronic polarization controller (EPC) with a maximum response time of 10 μs, which is a core component for polarization tuning, is controlled through 4 DC voltage channels. Since the transition dynamics mainly happens after the polarization tuning is completed so the response time of the EPC will not affect the transition dynamic of the fiber laser. Thus, by recording several sets of voltages that lead to the different operating regimes achieved using the intelligent algorithm, i.e., the previously experienced values, the laser can switch directly among multiple operating regimes. A 3 dB optical coupler retains half the power inside the cavity while the other half is for output. This output is sequentially divided by another optical coupler. The upper branch is used for the TS-DFT through a chirped fiber Bragg grating (FBG) with a dispersion value of −1651 ps/nm in the C band. Note, the spectrum width of the input is filtered down to 50 nm via the chirped FBG that has a rectangular spectral response over the range from 1525 nm to 1575 nm. In the lower branch, after photodetection, the left branch is sent to the intelligent feedback panel, consisting of an analogue-to-digital converter (ADC), a field-programmable gate array (FPGA), and 4 digital-to-analogue converters (DACs) for regime control, while the right branch is sent directly to the oscilloscope for real-time recording. The real-time oscilloscope operates at a sampling rate of 10 GSa/s indicating a spectral resolution of ∼0.06 nm, which is the result of the sampling interval divided by the absolute value of the dispersion. The cavity length of the fiber laser is ∼47.8 m giving a fundamental repetition rate of 4.325 MHz, which corresponds to a roundtrip time of approximately 0.23 μs and the dispersion of the laser cavity is 7.79 ps/nm/km. Note, to ensure successful acquisition of each transition, the FPGA is programmed to transmit a trigger signal to the oscilloscope immediately after the experienced voltages are loaded.

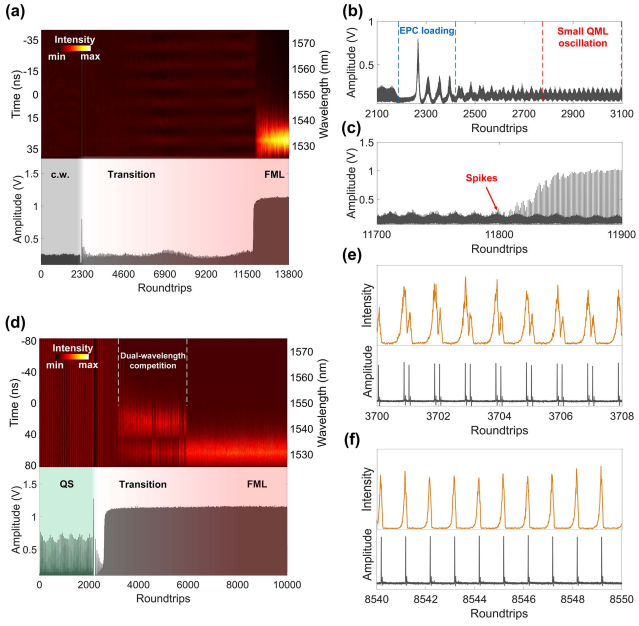

Fig. 2. Records of switching processes to the FML regime from the cw state and QS regime. (a)–(c) Records of switching from the cw state to the FML regime. (a) TS-DFT result (upper) and real-time waveform record (lower). (b) The initial part and c, the approaching part of the transition phase. (d)–(f) Records of switching from the QS regime to the FML regime. (d) TS-DFT result (upper) and real-time waveform record (lower). (e) Undispersed (lower) and dispersed pulses (upper) of the dual-pulse phenomenon. (f) Undispersed (lower) and dispersed pulses (upper) under FML regime.

III. Results and Discussion

A. Transition Dynamics to FML Regime From Continuous-Wave (cw) State and QS Regime

Figure 2(a) illustrates the switch from cw state (the initial noise fluctuations) to the FML regime based on loading of the previously experienced voltage value that corresponds to the FML regime into the EPC. From the TS-DFT results, the upper part of Fig. 2(a), some picosecond fluctuations oscillate rapidly and one of these oscillations eventually leads to mode locking. The obvious boundary in the TS-DFT result and the peak shown in the real-time record, the lower part of Fig. 2(a), around the 2300th roundtrip arise from the abrupt polarization change produced by the EPC, which is the sign that the experienced values have been loaded. The real-time record shows that the complete transition phase takes approximately 10000 roundtrips, from the 2300th to the 12300th roundtrip, which represents approximately 2.3 ms in our cavity; however, the time cost is rather random and ranges from several hundred microseconds to several milliseconds, even for the identical FML regime during multiple measurements. Different with our case, the time cost for the FML regime is similar for mode-locking by simply pump power increasing due to the different mode-locking mechanism. The initial phase of the transition is shown in Fig. 2(b). The EPC loading phase probes a sort of damped relaxation oscillation (pulsation with decreasing amplitude) [10]. After the previously experienced values have been loaded, the laser evolves into a small-amplitude QML-type oscillation, which is the temporal manifestation of superposition of multiple picosecond oscillations [6], and maintains this type of oscillation until it reaches the FML

regime. Figure 2(c) shows the dynamic when approaching the FML regime, where some spikes stand out in the small-amplitude QML-type oscillation. Apparently, these spikes trigger the onset of mode-locking.

Figure 2(d) illustrates the transition dynamics from QS to the FML regime. The TS-DFT results manifest in an intriguing dynamic after the EPC loading process, where there are initially two dominant wavelengths at 1531 nm and 1542 nm. Before the evolution into the FML regime, the power at the longer wavelength is obviously stronger than that at the shorter wavelength. However, the relationship flips immediately after entering the FML regime. In a sense, this phenomenon demonstrates competition between the dual wavelengths, where the shorter wavelength wins after the 6000th roundtrip, and the spectrum eventually stabilizes. To enhance our understanding of the dual-wavelength competition, we compared the undispersed and dispersed pulses during the competition, as shown in Fig. 2(e). Interestingly, the dual-wavelength competition situation corresponds to the dual-pulse phenomenon that occurs in the undispersed time domain, and the time interval between two closely-spaced pulses is only approximately one-fifth of a roundtrip. Obviously, the first peak outweighs the second peak in each dispersed pulse in the dual-pulse phenomenon. Because the chirped FBG applied in the TS-DFT has normal dispersion in the C-band, the higher peak corresponds to the longer wavelength, while the other peak corresponds to the shorter wavelength. This conclusion is identical to the TS-DFT results. Additionally, according to our multiple measurements, the dual-pulse phenomenon occurs randomly when switching to the FML regime from either the cw state or the QS regime. After the spectrum stabilizes, the dual-pulse phenomenon disappears and the laser operates in the stable FML regime, as indicated by Fig. 2(f). For comparison, the transition time from the QS regime to the FML regime is much shorter than that from the cw state to the FML regime. Note, different from the transition from cw state to the FML regime (only 1 chirped FBG used), 2 chirped FBGs with the same dispersion parameter are utilized. Thus, the equivalent dispersion parameter in the transition from QS regime to the FML regime is -3302 ps/nm giving a higher spectral resolution of $\sim$0.03 nm. Therefore, the corresponding temporal length from 1525 nm to 1575 nm is 165.1 ns.

B. Transition Dynamics to QS Regime From cw State and FML Regime

The transitions to the QS regime from both the cw state and FML regimes are recorded in Fig. 3(a) and (c), respectively. The TS-DFT is not quite effective on QS pulses. First, the QS spectrum width is generally narrower than that of the mode-locked pulses, and thus the pulse broadening phenomenon is less obvious. Second, the QS pulse width is much larger when compared with the amount of broadening produced by dispersion. Therefore, the transition analyses of switching to the QS regime are substantially reliant on time-domain records. Analogous to the switching process from the cw state to the FML regime, the laser enters the small-amplitude QML oscillation from both switches. Intriguingly, the period of the envelope of the small-amplitude QML oscillation is

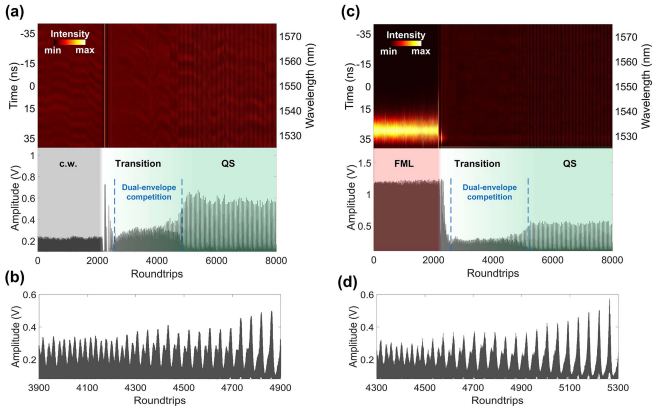

Fig. 3. Records of switching processes to the QS regime from the cw state and FML regime. (a)–(b) Records of switching from the cw state to the QS regime. (a) TS-DFT result (upper) and real-time record (lower). (b) Approaching part of the transition phase. (c)–(d) Records of switching from the FML regime to the QS regime. (c) TS-DFT result (upper) and real-time record (lower). (d) Approaching part of the transition phase.

almost half of the period of the QS regime. The dynamics when approaching the QS regime from the cw state and FML regimes, as illustrated by Fig. 3(b) and (d), respectively, are quite analogous. Since this process resembles a sort of competition between these two envelopes, we term it as dual-envelope competition. The damped relaxation oscillation induced by the EPC loading coexists with the emerging QS pulses forming the dual-envelope competition. With the further decrease of the damped relaxation oscillation, the dual-envelope competition disappears and the QS regime is finally reached. This peculiar dynamic is also observed in massive switches from different operating regimes or from cw state to the QS regime. The transition dynamics and time costs from cw state and FML regime to the QS regime are almost the same.

C. Transition Dynamics Between FML Regime and Higher-Order HML Regimes

The transitions between the FML and higher-order HML regimes are also recorded. The transition phase of the real-time record in Fig. 4(b) shows that the transition is completed rapidly, within only 300 roundtrips. Note, the essential spikes are also observed during the transition phase, thus proving that the mode-locking originates from the spikes that occur inside the QML oscillations. Nevertheless, the spectrum width gradually narrows and ultimately settles down at approximately the 7000th roundtrip, as indicated by the TS-DFT results shown in the upper part of Fig. 4(a). The undispersed and dispersed pulses before the spectrum is stabilized are shown in Fig. 4(c). While the undispersed pulses show stable temporal characteristics in the second-order HML regime, the dispersed pulses are distorted and contain numerous spikes, corresponding to a broad and unstable optical spectrum. Figure 4(d) shows the undispersed and dispersed pulses after the spectrum stabilized. When compared with the pulses before the spectrum stabilized, the time-domain pulses show little difference, but the dispersed pulses are far smoother and more stable after the spectrum is stabilized. Combining the TS-DFT results with the real-time

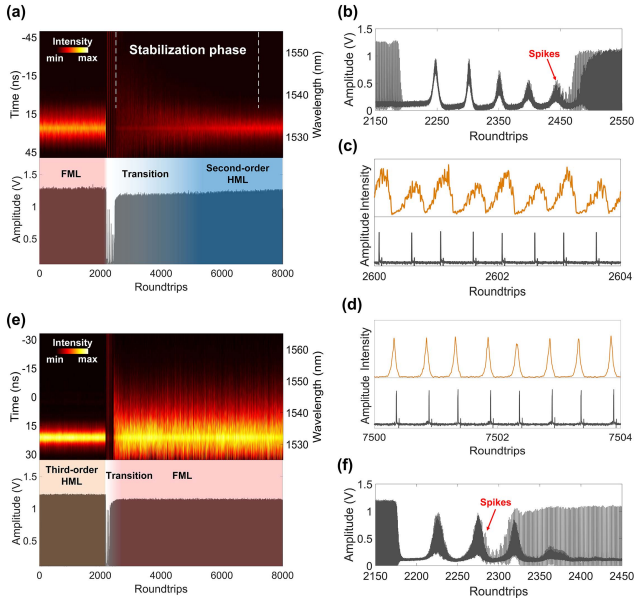

Fig. 4. Records of switching from the FML regime to the second-order HML regime and switching from the third-order HML regime to the FML regime. (a)–(d) Records of switching from the FML regime to the second-order HML regime. (a) TS-DFT result (upper) and real-time record (lower). (b) Transition phase. The undispersed (lower) and dispersed pulses (upper) (c) before and (d) after the spectrum stabilizes. (e)–(f) Records of switching from the third-order HML regime to the FML regime. (e) TS-DFT result (upper) and real-time record (lower). (f) Transition phase.

recording allows us to conclude that the transition from FML to the higher-order FML regimes will require a long time to stabilize. It should be noted that 2 chirped FBGs are applied in the transition from the FML regime to the second-order HML regime. However, certain parts of dispersed pulses (from 1525 nm to 1555 nm) are extracted and demonstrated owing to the overlap between dispersed pulses.

Figure 4(e) shows that the transition from the third-order HML regime to the FML regime is much more direct. There is barely a transition phase from both the TS-DFT results and the real-time record shown in Fig. 4(e). However, the spectrum bandwidth broadens rapidly when transiting to the FML regime. Figure 4(f) shows the transition dynamics in detail, from which it is obvious that the spikes that trigger the FML regime appear during the EPC loading phase and then evolve into a stable FML regime. The switching time from the higher-order HML to the FML regime is of the order of only tens of microseconds, which is much faster than switching from the FML regime to a higher-order HML regime and is the fastest switching time among the observations. Therefore, we can conclude that the evolution from the regime with lower stability (i.e., the HML regime) to that with higher stability (i.e., the FML regime) is much smoother than the reverse transition, which agrees well with the physical evolution mechanism. Note, the overlap between pulses still exists due to the higher repetition of the third-order HML regime. Hence, analogous to the previous transition, parts of dispersed pulses (from 1525 nm to 1565 nm) are exhibited here.

IV. Conclusion

In conclusion, we first unveiled the dynamics of direct switching among multiple operation regimes by virtue of the use of a homemade real-time programmable MLFL [15]. As a result of the insight gained into the regime transition dynamics, we have observed some interesting phenomena that have not been reported previously. The mode-locking behaviour always originated from the spikes that were observed in the small QML oscillations, regardless of whether the transition was from the cw state or QS regime. The regime transition from QS to the FML regime will occasionally experience dual-wavelength competition. On the other hand, dual-envelope competition always exists and only the dominant pulse can eventually be oscillated for the QS pulse build-up process, no matter whether the transition is from the cw state or FML regime. The transition time from the HML regime with lower stability to the FML regime with higher stability is much shorter than the reverse process and only requires tens of microseconds, which is the fastest regime transition time reported to date. We believe that these findings can enrich the wider understanding of the complex nonlinear dynamics of MLFLs and provide new insights for fiber laser design and applications.

References

[1] J. Kim and Y. Song, "Ultralow-noise mode-locked fiber lasers and frequency combs: Principles, status, and applications," *Adv. Opt. Photon.*, vol. 8, no. 3, pp. 465–540, Sep. 2016.

[2] A. S. Bhushan, F. Coppinger, and B. Jalali, "Time-stretched analogue-to-digital conversion," *Electron. Lett.*, vol. 34, no. 9, pp. 839–841, Apr. 1998.

[3] A. Mahjoubfar, D. V. Churkin, S. Barland, N. Broderick, S. K. Turitsyn, and B. Jalali, "Time stretch and its applications," *Nature Photon.*, vol. 11, pp. 341–351, Jun. 2017.

[4] C. Lecaplain, P. Grelu, J. M. Soto-Crespo, and N. Akhmediev, "Dissipative rogue waves generated by chaotic pulse bunching in a mode-locked laser," *Phys. Rev. Lett.*, vol. 108, Jun. 2012, Art. no. 233901.

[5] A. F. J. Runge, N. G. R. Broderick, and M. Erkintalo, "Observation of soliton explosions in a passively mode-locked fiber laser," *Optica*, vol. 2, no. 1, pp. 36–39, 2015.

[6] G. Herink, B. Jalali, C. Ropers, and D. R. Solli, "Resolving the build-up of femtosecond mode-locking with single-shot spectroscopy at 90 MHz frame rate," *Nature Photon.*, vol. 10, no. 5, pp. 321–326, Mar. 2016.

[7] X. Wei, B. Li, Y. Yu, C. Zhang, K. K. Tsia, and K. K. Y. Wong, "Unveiling multi-scale laser dynamics through time-stretch and time-lens spectroscopies," *Opt. Express*, vol. 25, no. 23, pp. 29098–29120, 2017.

[8] H.-J. Chen *et al.*, "Buildup dynamics of dissipative soliton in an ultrafast fiber laser with net-normal dispersion," *Opt. Express*, vol. 26, no. 3, pp. 2972–2982, 2018.

[9] P. Ryczkowski, M. Närhi, C. Billet, J.-M. Merolla, G. Genty, and J. M. Dudley, "Real-time full-field characterization of transient dissipative soliton dynamics in a mode-locked laser," *Nature Photon.*, vol. 12, no. 4, pp. 221–227, 2018.

[10] X. Liu, X. Yao, and Y. Cui, "Real-time observation of the buildup of soliton molecules," *Phys. Rev. Lett.*, vol. 121, no. 2, Jul. 2018, Art. no. 023905.

[11] S. Sun, Z. Lin, W. Li, N. Zhu, and M. Li, "Time-stretch probing of ultra-fast soliton dynamics related to Q-switched instabilities in mode-locked fiber laser," *Opt. Express*, vol. 26, no. 16, pp. 20888–20901, 2018.

[12] M. S. Kang, N. Y. Joly, and P. S. J. Russell, "Passive mode-locking of fiber ring laser at the 337th harmonic using gigahertz acoustic core resonances," *Opt. Lett.*, vol. 38, no. 4, pp. 561–563, 2013.

[13] Y. Chen *et al.*, "Mechanically exfoliated black phosphorus as a new saturable absorber for both Q-switching and mode-locking laser operation," *Opt. Express*, vol. 23, no. 10, pp. 12823–12833, 2015.

[14] L. C. Kong *et al.*, "Passive Q-switching and Q-switched mode-locking operations of 2 Âμm Tm:CLNGG laser with MoS_2 saturable absorber mirror," *Photon. Res.*, vol. 3, no. 2, pp. A47–A50, 2015.

[15] G. Pu, L. Yi, L. Zhang, and W. Hu, "Intelligent programmable mode-locked fiber laser with a human-like algorithm," *Optica*, vol. 6, no. 3, pp. 362–369, 2019.